ISSN 1063-7710, Acoustical Physics, 2019, Vol. 65, No. 2, pp. 226–233. © Pleiades Publishing, Ltd., 2019.

ACOUSTIC SIGNALS PROCESSING. COMPUTER SIMULATION

Subarray Beam-space Adaptive Beamforming Combined with Array Shape Estimation based on Non-Acoustic Sensor[1]

Q. Wang[a, b, *], B. Zhou[a, b], Y. Chen[a, b], and H. Quan[a, b]

[a] *Science and Technology on Sonar Laboratory, Hangzhou, China*

[b] *Hangzhou Applied Acoustics Research Institute, Hangzhou, China*

**e-mail: wangqing2015019@163.com*

Received March 22, 2018; revised September 27, 2018; accepted October 30, 2018

Abstract—To address the issue of serious decline in performance of the array signal processing caused by the towed array shape distortion during maneuvering, this paper presents a new method of subarray beam-space adaptive beamforming combined with an array shape estimation method based on non-acoustic sensor. Firstly, the array shape through the approximate circular arc structure of the array segment between the adjacent sensor during maneuvering is preliminary calculated. Next, the final estimated array shape through a smooth processing method on the entire array shape by means of a calibration method using spline interpolation technique is achieved. This method is able to estimate the array shape in real time. The array steering vector based on the real-time estimation of the array shape is updated, using a subarray beam-space adaptive beamforming (SBABF) to reduce the demand of the number of the snapshots. And the beam-space covariance matrix converges fast within a few snapshots. The SBABF method combined with array shape estimation (AE-SBABF) was verified by simulation data and sea trial data processing results. During maneuvering, the AE-SBABF can not only improve the array processing gain of the target effectively, but also solve the left/right ambiguity problem well.

Keywords: array shape estimation, non-acoustic sensor, spline interpolation technique, subarray beam-space adaptive beamforming

DOI: 10.1134/S1063771019020106

1. INTRODUCTION

Horizontal flexible towed arrays have been widely used in sonar equipment because of their advantages, such as low operating frequency range, large array aperture, and long range [1]. However, in the actual marine environment, platform maneuvers, internal waves, surges, etc. can cause array distortion. In the case of maneuvering, the existing array signal processing methods are often processed in a horizontal linear array, resulting in degraded detection performance [2, 3]. Especially for high-resolution adaptive processing algorithms, the detection performance will be seriously affected [4, 5]. Therefore, it is necessary to estimate the shape of the towed array during the maneuvering. There are two main categories of array shape estimation methods: acoustic calculation methods and non-acoustic aided measurement methods. The acoustic calculation method is usually based on the condition that the auxiliary sound source is a narrowband signal and a far-field plane wave, and the requirement on the signal-to-noise ratio is high [6, 7]. The limitations of this kind of method make it unable to adapt to the needs of combat mobility and real-time performance. Non-acoustic array assisted measurement methods are commonly used in two ways. The one is to use hydrodynamic methods to estimate through analyzing the force condition of the towing cable microelement [8–10]. This method is computationally intensive and has an estimated decrease in performance during maneuvering. Another method of non-acoustic array measurement mainly relies on the information acquired by equipment such as heading, depth and pressure sensors installed at specific positions of the tow array to estimate the array shape [11–14], which can effectively avoid the limitations of acoustic calculation methods and can be estimated in real time.

The array element space adaptive beamforming method using the inverse of the covariance matrix requires long snapshot data to ensure the full rank of the covariance matrix. When the maneuvering state of the towed array rapidly changes, the array pattern of its relative target also changes during an adaptive processing cycle, and the target signal is decomposed into multiple feature vectors in the array covariance matrix of the array element, which causes the signal to be mismatched in the following beamforming. Its energy is decomposed into multiple eigenvalues, which results in a decrease in processing gain [15]. However,

[1] The article is published in the original.

the subarray beam-space adaptive beamforming (SBABF) method first pre-forms multiple beams through conventional beamforming. The sensitivity of conventional beamforming to steering vector mismatch is much lower than that of adaptive beamforming, and it has certain robustness [16]. In addition, the SBABF method achieves fast convergence of the beam-space covariance matrix with fewer snapshot data by reducing the dimension. It is suitable for situations where the target or local sonar platform is fast maneuvering and other sources have short coherence time. The SBABF method reduces adaptive algorithm's requirement on the number of snapshots and improves the convergence speed of covariance matrix estimation [17, 18].

Based on the above two points, this paper proposed a subarray beam-domain adaptive beamforming method combined with non-acoustic sensor array estimation (AE-SBABF). This method can update array patterns in real time based on the array estimation results, and then perform subarray adaptive beamforming, which can reduce the loss of signal mismatch and processing gain.

2. ARRAY SHAPE ESTIMATION METHOD BASED ON NON-ACOUSTIC SENSOR

Considering that, it is difficult for a flexible towed array between two adjacent sensors in an actual marine environment to maintain a straight line, and it is impossible to bend the higher-order curve. Therefore, this paper proposes to estimate the arrays between each two sensor arrays and use circular arcs to represent the arrays between two non-acoustic sensor nodes.

The heading sensor is located at the center position between the array elements and used for sensor spacing. Suppose that the number of elements in the towed array is N, the number of subarrays is M and the number of elements in subarray is n. The array elements are evenly arranged between the two sensors with the number of n, and the array element spacing is denoted as d. Figure 1 shows the array of arc structures between two sensors on the towed array. The previous sensor position is the coordinate origin and the tangential direction is the X-axis direction. Then use the difference of the heading angle of the front and rear sensors to unite the coordinate system. Figure 2 shows the relative positional relationship between the sensors. The following is the theoretical derivation of the coordinate transformation.

As shown in Fig. 1, the first sensor (heading angle θ_1) position is used as the origin of coordinates, and the tangential direction is the X-axis direction. The second sensor heading angle is θ_2, and $\Delta\theta = \theta_2 - \theta_1$. The array between two sensors can be approximated as a circular structure. It can be known from the geometric relations that the angle corresponding to the arc denotes $\theta = \Delta\theta$. The radius of the arc is $R = nd/\Delta\theta$.

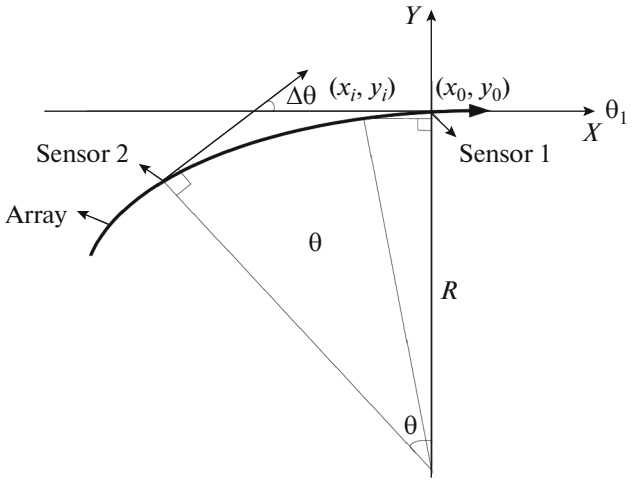

Fig. 1. The shape of the horizontal flexible line array during maneuvering.

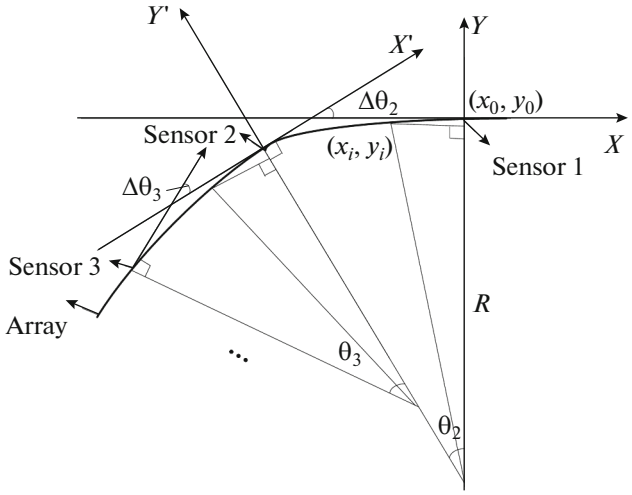

Fig. 2. The relative position of different array segments.

With the first array element coordinates as the origin, the position of the second array element is

$$\begin{aligned} x_2 &= -R_1 \sin(\Delta\theta/n), \\ y_2 &= -R_1[1 - \cos(\Delta\theta/n)]. \end{aligned} \tag{1}$$

In a similar way, we find the position of the i-th array element:

$$\begin{aligned} x_i &= -R_1 \sin[(i-1)\Delta\theta/n], \\ y_i &= -R_1 + R_1 \cos[(i-1)\Delta\theta/n]. \end{aligned} \tag{2}$$

Similarly, as shown in Fig. 2, each two sensors use the corresponding sensor position as the origin of coordinates, and the heading is in the direction of the X-axis to establish the coordinate system.

According to the above method, the position of the array element between each sensor in the corresponding coordinate system can be obtained separately. After finding the position of each element between the last sensor, let us rotate it to the coordinate system with

respect to the origin where the previous sensor is located. The rotation formula is as follows:

$$\begin{bmatrix}\mathbf{x}'\\ \mathbf{y}'\end{bmatrix}=\begin{bmatrix}\cos\theta & -\sin\theta\\ \sin\theta & \cos\theta\end{bmatrix}\begin{bmatrix}\mathbf{x}\\ \mathbf{y}\end{bmatrix}, \quad (3)$$

where $(\mathbf{x},\mathbf{y})$ is the positions of the n elements in the original coordinate system, $(\mathbf{x},\mathbf{y})=(x_i,y_i)$, $i=1,2,\ldots,n$. $(\mathbf{x}',\mathbf{y}')$ is the positions of the n elements under the new coordinate system after rotation, and θ is the counterclockwise rotation direction, $(\mathbf{x}',\mathbf{y}')=(x_i',y_i')$, $i=1,2,\ldots,n$.

Since two arrays—the front and the rear one—share a sensor, they need to be translated when rotated to a new coordinate system. The translation formula is as follows:

$$\begin{cases}\mathbf{x}''=\mathbf{x}'+x_{\text{sensor}},\\ \mathbf{y}''=\mathbf{y}'+y_{\text{sensor}},\end{cases} \quad (4)$$

where $(\mathbf{x}'',\mathbf{y}'')$ is the positions of each array element in the array segment between the current sensor relative to the coordinate system of the previous array segment, $(\mathbf{x}'',\mathbf{y}'')=(x_i'',y_i'')$,$i=1,2,\ldots,n$.

By analogy, the positions of all the segments relative to the coordinate system of the first segment can be obtained, and then the calculated array shape can be obtained, denoted as $(\tilde{x}_m,\tilde{y}_m)$,$m=1,2,\ldots,N$, where, N denotes the total number of array elements.

Due to the towing maneuvering of the tugboat in the actual marine environment, the horizontal flexible towed array is often considered smooth. After obtaining the calculated array, the polynomial fitting technique (5th order) needs to be used to smooth the entire computing array. The spline-based calibration technique is used for constant array spacing.

That is, under the premise of horizontal equal spacing (d) between array elements, polynomial fitting is performed on the element position of the calculated array to obtain the smooth array shape. Use the spline interpolation method on the smooth array shape to obtain the interpolation points $(\tilde{x}_j,\tilde{y}_j)$, $j=1,2,\ldots,J$ where $J\gg N$. Select the interpolation point closest to the real array element position among the spline interpolation points $(\tilde{x}_j,\tilde{y}_j)$, that is, the closest to the array element spacing d among the interpolation points:

$$(x_m,y_m)_{sp}=\min\left|md-\sum_{j=1}^{p}\sqrt{(\tilde{x}_j-\tilde{x}_{j-1})^2+(\tilde{y}_j-\tilde{y}_{j-1})^2}\right|, \quad (5)$$

where $(x_m,y_m)_{sp}$ denotes the position of the final estimated m^{th} array element, $m=1,\ldots,N-1$, $j=1,2,\ldots,J-1$.

For each m, by continuously increasing the size of p, the position of the array element is selected in the interpolation point, so that the value of the above formula is minimized. All the positions of the array elements are calculated in turn, to obtain the entire estimated array.

3. SUBARRAY BEAM-SPACE ADAPTIVE BEAMFORMING COMBINED WITH ARRAY SHAPE ESTIMATION (AE-SBABF)

The AE-SBABF method first updates the array pattern for each snapshot based on the estimated array shape. The range-focus steering vector of the m^{th} subarray is as follows:

$$\mathbf{A}_m(r,t)=\frac{1}{\sqrt{N}}\left[e^{i\varphi_1(t)}\ \ e^{i\varphi_2(t)}\ \ \ldots\ e^{i\varphi_N(t)}\right], \quad (6)$$

where N denotes the number of array elements, $\varphi_n(t)=2\pi f\left|r-r_n(t)\right|/c$, c denotes the speed of sound, f denotes the frequency, $r_n(t)$ denotes the position of the estimated array element.

Subarray conventional beamforming is then performed to convert the array element space sampling matrix into a beam-space sampling matrix. The m^{th} subarray array element space sampling matrix is

$$\mathbf{X}_m(t)=\left[x_1(t)\ \ x_2(t)\ \ \ldots\ \ x_N(t)\right], \quad (7)$$

where $x_i(t)$ denotes the wave field data received by the i^{th} array element, $i=1,\cdots,N$.

The converted beam space sampling matrix is

$$\mathbf{B}(r,t)\big|_{M\times t}=\left[b_1(t)\ \ b_2(t)\ \ \ldots\ \ b_M(t)\right], \quad (8)$$

where M is the number of subarrays, and $b_m(t)$ is the conventional beamforming response at the m^{th} subarray and snapshot t, "H" denotes Hermitian transpose, as in formula (9), and $m=1,2,\ldots,M$.

$$b_m(t)=\mathbf{A}_m(r,t)^{\mathrm{H}}\cdot\mathbf{X}_m(t). \quad (9)$$

Then obtain the beam-space covariance matrix:

$$\mathbf{R}\big|_{M\times M}=\mathbf{B}(r,t)\cdot\mathbf{B}(r,t)^{\mathrm{H}}, \quad (10)$$

where, as in reference [12], only when the number of snapshot t is not less than twice the number of subarrays, the beam-space covariance matrix is full rank.

Then singular value decomposition for beam-space covariance matrix:

$$\mathbf{R}\big|_{M\times M}=\mathbf{V}^{\mathrm{H}}\big|_{M\times M}\cdot\mathbf{\Lambda}\big|_{M\times M}\cdot\mathbf{U}\big|_{M\times M}. \quad (11)$$

$\mathbf{\Lambda}$ is a diagonal matrix, the diagonal elements λ_i are called the singular values:

$$\mathbf{\Lambda}=\begin{bmatrix}\lambda_1 & 0 & \cdots & 0\\ 0 & \lambda_2 & \cdots & 0\\ \vdots & \vdots & \ddots & \vdots\\ 0 & 0 & \cdots & \lambda_M\end{bmatrix}. \quad (12)$$

$\mathbf{V}$ and $\mathbf{U}$ denotes the left singular vector and right singular vector respectively. The matrix $\mathbf{R}$ is a sym-

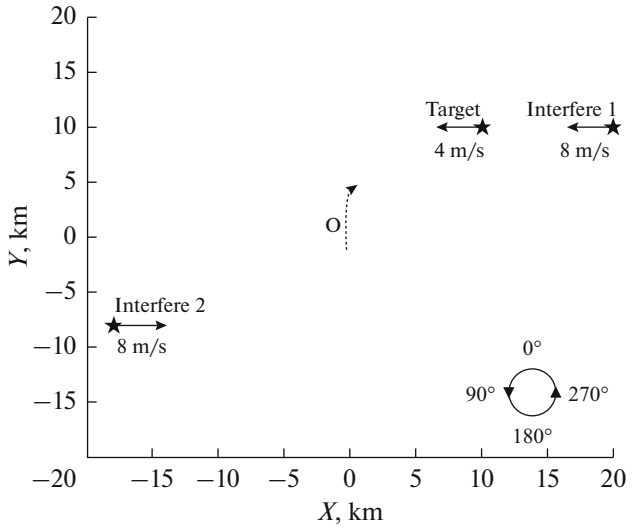

Fig. 3. The target situation.

metric square matrix, the left singular vector $\mathbf{V}$ and the right singular vector $\mathbf{U}$ are the same and

$$\mathbf{V} = [\mathbf{V}_1 \ \mathbf{V}_2 \ \ldots \ \mathbf{V}_M]. \tag{13}$$

The vector $\mathbf{V}_m$ is M multiplying 1-dimension, $m = 1, 2, \ldots, M$.

The inverse of the beam-space sampling matrix after diagonal loading can be obtained as follows:

$$\mathbf{R}^{-1}\big|_{M\times M} = \sum_{m=1}^{M} \frac{1}{\lambda_m + \varepsilon} \mathbf{V}_m \mathbf{U}_m{}^{\mathrm{H}}, \tag{14}$$

where ε is the diagonal load of the sampling matrix.

Finally, the beam direction output is obtained by matching with a uniform vector. The weight vector of the subarray adaptive beamforming and the spatial spectrum estimation result of the subarray adaptive beamforming are obtained:

$$\mathbf{W}_b\big|_{M\times 1} = \frac{\mathbf{R}^{-1}\mathbf{1}}{\mathbf{1}^{\mathrm{H}}\mathbf{R}^{-1}\mathbf{1}}, \tag{15}$$

$$\mathbf{P}_{\mathrm{AE\_SBABF}} = \mathbf{W}_b^{\mathrm{H}}\mathbf{R}\mathbf{W}_b. \tag{16}$$

The beam-space covariance matrix has a lower order rank than the array element space covariance matrix, so this method can have more stable estimation performance in a few snapshots. Whereas the MVDR method requires snapshot data that is more than twice the number of array elements to make the array element space covariance matrix of full rank. For array compensation in the maneuver state, the dispersion of the eigenvalues of the signal in the beam domain can be more effectively reduced, thereby reducing the loss of signal mismatch and processing gain.

4. SIMULATION RESULTS

Consider a 256-element towed array with 300 Hz half-wavelength arrays, and towed array deflected eastward in the north-east direction with a 15 degree arc angular array. The drag speed is 5 m/s, the north direction is the *Y*-axis, the first array element is the origin, and the *XOY* coordinate system is constructed. The target signal is located on the starboard side (10000, 10000 m) point and moves in the positive west direction at a speed of 4 m/s, radiating a 300 Hz narrowband signal with a signal-to-noise ratio of −10 dB. The two equal power interferences are located on the starboard side (20000, 10000 m) and the port side (−18000, −8000 m) of the array. They are respectively 8 m/s to the west and the east direction, each radiating a 300 Hz narrowband signal, and the interference and noise

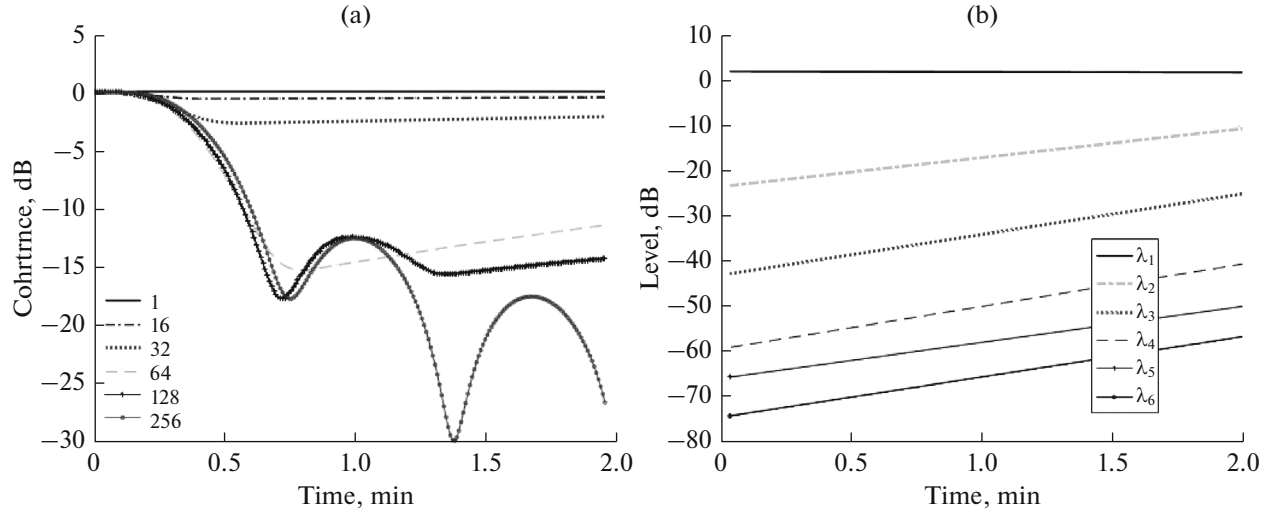

Fig. 4. Signal correlation analysis between arrays. (a) The correlation coefficient between the first array element and the related array element changes with time, (b) signal eigenvalues expansion over time.

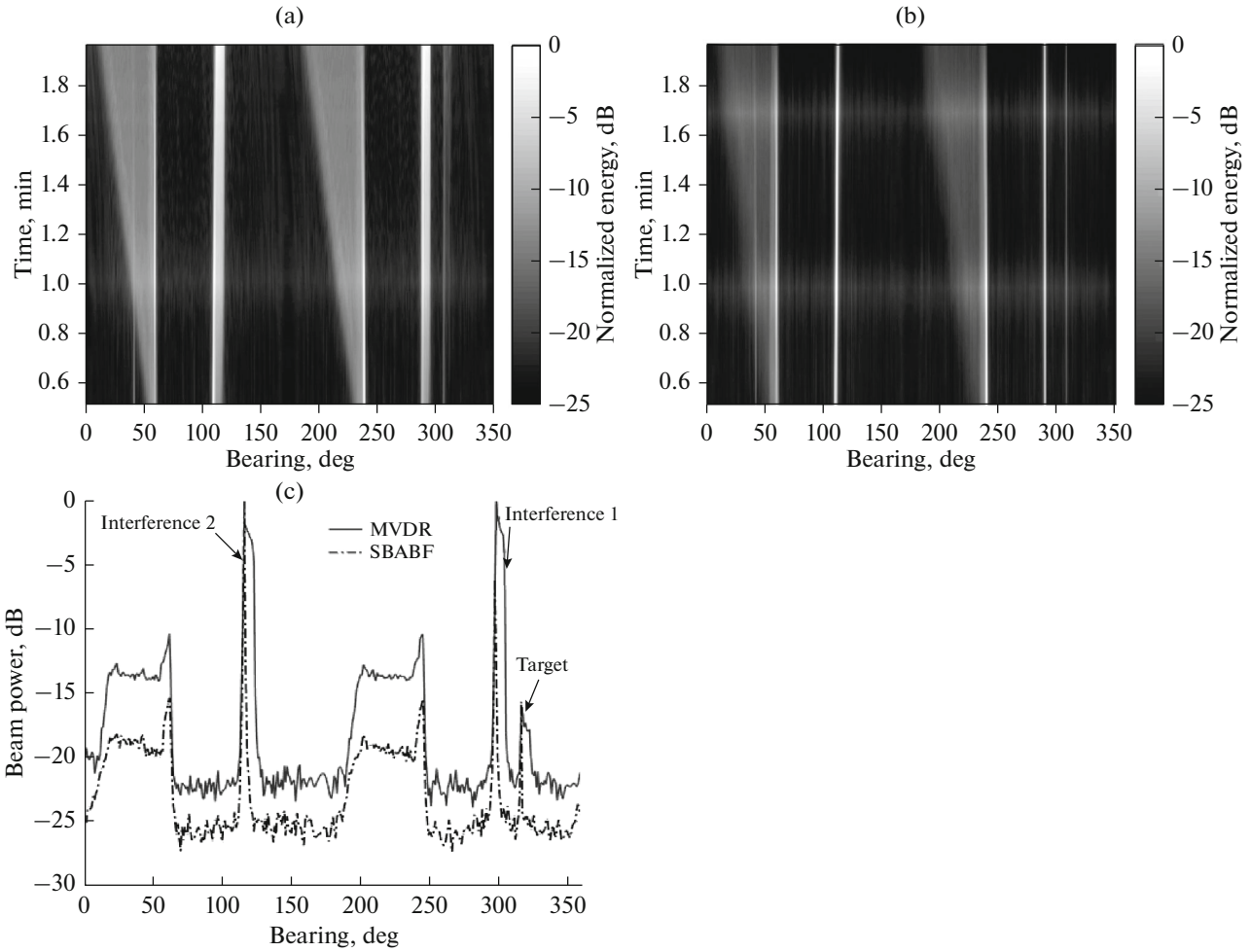

Fig. 5. MVDR-DL and SBABF processing results with array shape fully known. (a) Time and bearing result of MVDR-DL, (b) time and bearing result of SBABF, (c) comparison of processing results for a snapshot at time 1.25 min.

ratio is 10 dB, the noise is random space white noise, and the power is 0 dB. The schematic diagram of the target situation is shown in Fig. 3.

The signal correlation [12] between the first array element and the 16, 32, 64, 128, and 256 array elements calculated with 60 snapshots (0.5 seconds per snapshot) under pure signal conditions is given as Fig. 4. It can be seen that the signal correlation between the array elements declines as the array bow angle changes. The farther apart the array elements are from each other, the worse the correlation of the array signals. This correlation loss is mainly caused by the relative motion between the target and the array. This kind of correlation loss is also caused by the expansion of signal eigenvalues. The specific expansion is shown in Fig. 4b.

Figure 5 shows the power output of MVDR-DL (Minimum Variance Distortionless Response-Diagonal Loading) diagonally loaded with 3 dB and adaptive beamforming of the subarray beam-field in the case where the array shape is fully known. Figures 5a, 5b are the entire time histograms, and Fig. 5c is a slice diagram of 60 snapshots processing results at time points of 1.25 minutes, where the straight line represents the processing result of MVDR-DL and the dot-dashed line represents the result of SBABF.

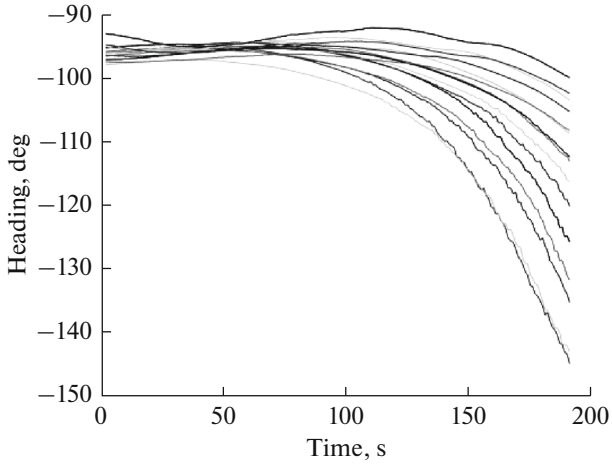

Fig. 6. Heading sensor data collected from a sea trial.

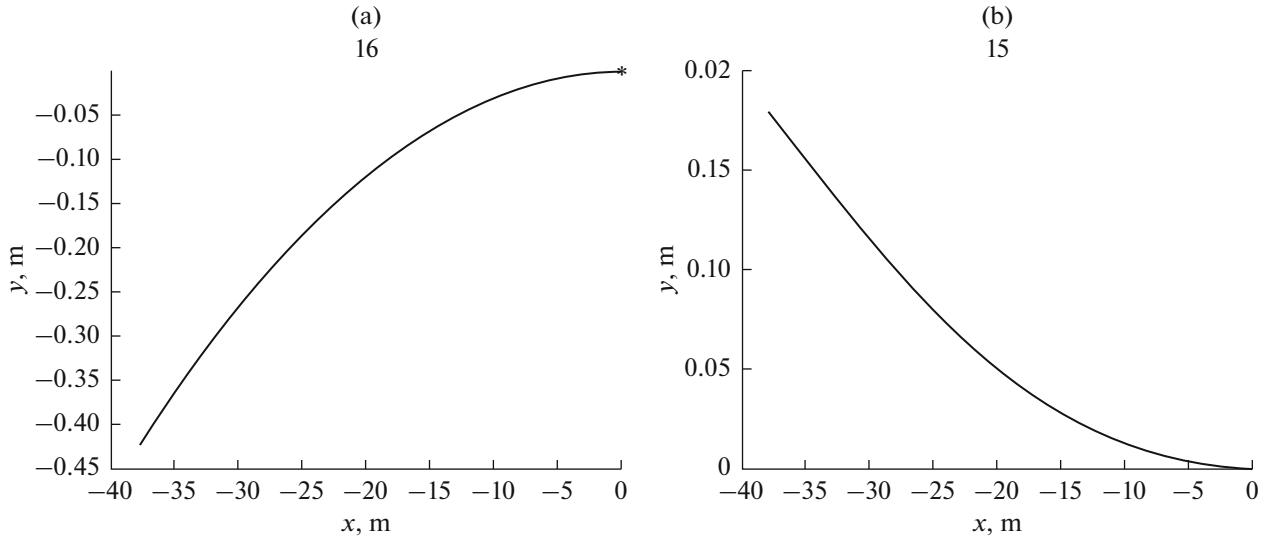

Fig. 7. The array position calculated by two segments. (a) The coordinates of the calculated 16th array, (b) the coordinates of the calculated 15th array.

As it can be seen from the figure, in the case of fully identified array shape, the SBABF can not only detect the target signal, but also achieve the port/starboard discrimination of the target, and the beam width is significantly narrower than that of the MVDR-DL. The output SNR detected in Fig. 5c is 2 dB higher than the diagonally loaded MVDR-DL. The port/starboard discrimination capability is due to large target image beam background interference, and cannot be fully accurately resolved throughout the entire time period, but the overall SBABF port/starboard discrimination capability is better than that of diagonally loaded MVDR's port/starboard discrimination.

5. PROCESSING RESULTS OF THE EXPERIMENT DATA

Combining real heading sensor data, the method for the above estimating array shape method is specifically explained. The experimental sea area is in a certain area of the South China Sea with a depth of about 100 meters and the towed ship's speed is 3 meters per second. The aperture of the array is 306 meters. The processing frequency meets the half-wavelength condition. The moving speed of the target is 2 m/s with a signal-to-noise ratio of −10 dB. The bearing angle is from 98° to 90°. The interference is unknown far-field interference and other non-cooperative fishing vessel interference. The towed array is evenly distributed with 256 array elements. The whole array is divided into 16 subarrays, and the number of subarray elements is 16.

Figure 6 shows the heading sensor data on a towed array collected by a sea trial test. The horizontal axis is the sampling time, and the vertical axis is the heading sensor data. It can be seen that the platform begins to maneuver around 100 s. Non-acoustic sensor data is filtered to remove outliers.

Then we calculate the position of array elements according to the circular arc structure. We take the location of the array elements in the 15th and 16th array segment as an example. Figure 7a is the position of each element of the 16th array in the coordinate system calculated from the bow structure, and Fig. 7b is the position of each element of the 15th array calculated in the coordinate system. According to the rotation formula, the position of each array element in the 15-block segment is calculated as shown in Fig. 8.

The array segments are rotated to the coordinate system of the first array segment. So we obtain the initial calculation array shape, and then the entire array is

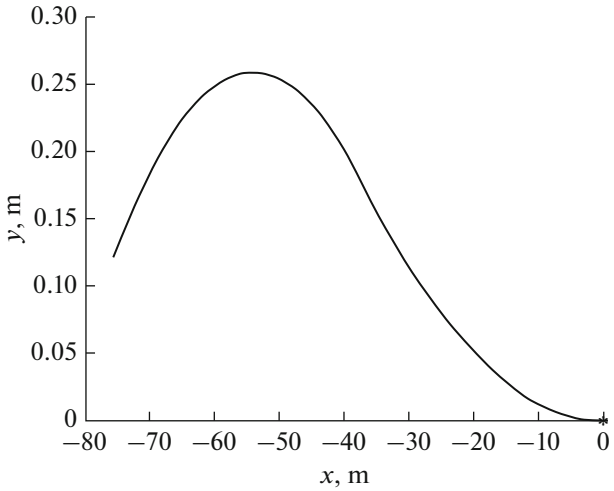

Fig. 8. 16-segment rotation to 15-segment coordinate system.

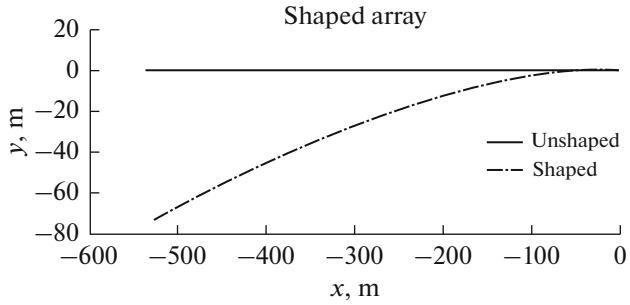

Fig. 9. Array estimation results. The straight line represents the linear array. The dot-dashed line represents the array shape estimation method proposed in Section 2.

smoothed using the spline interpolation calibration technique. Figure 9 shows the results of a certain batch array shape estimation result when the tug is maneuvered. The straight line denotes the horizontal linear array, and the dot-dashed line denotes the estimated array shape based on the array shape estimation method proposed by this paper in Section 2. It can be seen that the estimated array shape by this method is closer to the true shape of the towed array during maneuvering.

Array signal processing on the sea trial data is based on the estimated formation with CBF (Conventional Beamforming), MVDR (Minimum Variance Distortionless Response), and AE-SBABF algorithms. Under half-wavelength conditions, the AE-SBABF algorithm uses 256 array elements, 64 frequency domain snapshots, and the whole array is divided into 16 subarrays, and the number of subarray elements is 16. From the processing results in Figs. 10 and 11, it can be concluded that the AE-SBABF algorithm has interference suppression performance relative to conventional beamforming and has a higher output SNR gain than MVDR, as shown in Fig. 1. The target output signal to noise ratio increased by 2.94 dB, as shown

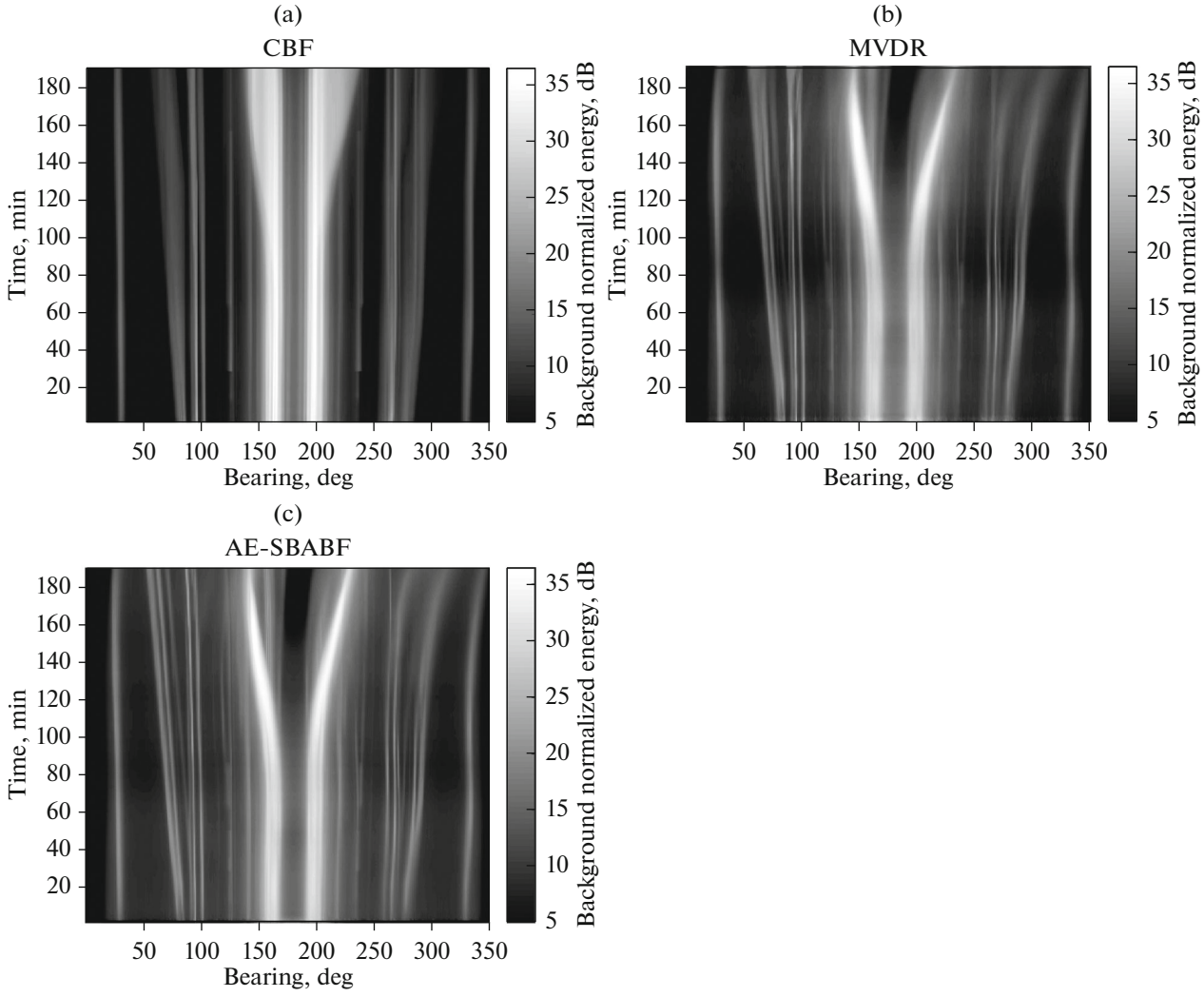

Fig. 10. Sea trial data processing results. (a) CBF, (b) MVDR, (c) AE-SBABF.

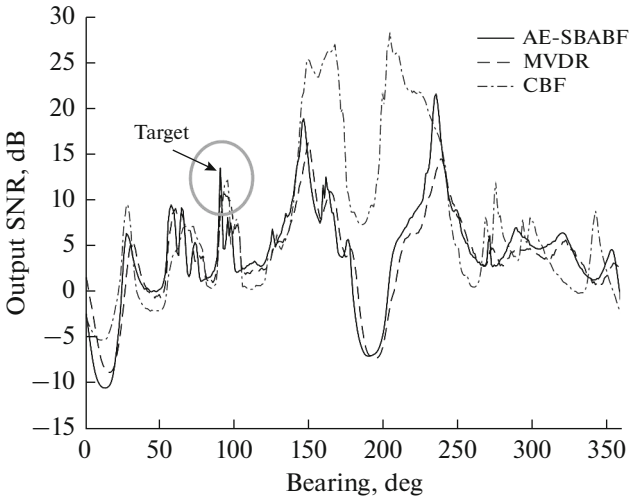

Fig. 11. Comparison of the results of different algorithms. The straight line represents the result of AE-SBABF, the dashed line represents the result of MVDR, the dot-dashed line represents the result of CBF (the target has been marked in the ellipse box).

in the circle. At the same time, from the MVDR and AE-SBABF processing results, it can be seen that the straight-ahead target trajectory will not be steered due to the turning of the platform, and the starboard target can be visually recognized through the widening of the target beam width and the azimuth rate of change.

6. CONCLUSIONS

This paper proposes a subarray beam-space adaptive beamforming method combined with array shape estimation based on non-acoustic sensor. The algorithm can achieve real-time estimation of distortion array shape under approximate bow structure based on horizontal flexible towed array segment and spline interpolation calibration technique during maneuvering. Array patterns are updated in real time based on the estimated array shape, and a subarray beam-space adaptive beamforming method with stable estimation performance in a few snapshots is adopted. Simulation data processing and actual sea trial data processing results verify this method. The target's processing gain can be effectively improved when the platform is maneuvered. Compared with the MVDR, the processing gain is increased by more than 2 dB, and the starboard target can be visually recognized through the widening of the target beam width and the azimuth rate of change, which has a very good engineering application value.

ACKNOWLEDGMENTS

This study was founded by Young Elite Scientists Sponsorship Program by CAST (Grant no. 2017QNRC001) and the National Natural Science Foundation of China (Grant no. 61701450).

REFERENCES

1. V. A. Zverev and P. I. Korotin, Acoust. Phys. **61** (6), 724 (2015).
2. W. S. Hodgkiss, IEEE J. Oceanic Eng. **8** (3), 120 (1983).
3. D. M. Caveny, D. R. D. Balzo, J. Leclere, and G. E. Loup, J. Acoust. Soc. Am. **80** (4), 2203 (1998).
4. N. Ma and J. T. Goh, Oceans **3** (1), 1895 (2000).
5. G. S. Malyshkin, A. S. Kuznetsova, and G. B. Sidel'nikov, Acoust. Phys. **62** (2), 235 (2016).
6. B. G. Ferguson, D. A. Gray, and J. L. Riley, J. Acoust. Soc. Am. **91** (3), 1565 (1992).
7. J. J. Smith, Y. H. Leung, and A. Cantoni, IEEE Trans. Signal Process. **44** (4), 1033 (1996).
8. J. L. Riley and D. A. Gray, IEEE J. Oceanic Eng. **18** (4), 572 (1993).
9. J. L. Odom and J. L. Krolik, IEEE J. Oceanic Eng. **40** (2), 465 (2015).
10. F. Lu, E. Milios, S. Stergiopoulos, and A Dhanantwari, IEEE J. Oceanic Eng. **28** (3), 552 (2003).
11. P. Felisberto, S. M. Jesus, IEE Proc.–Radar, Sonar Navig. **143** (3), 210 (1996).
12. P. Gerstoft, W. S. Hodgkiss, W. A. Kuperman, H. Song, M. Siderius, and P. L. Nielsen, IEEE J. Oceanic Eng. **28**(1), 44 (2003).
13. H. Y. Park, D. H. Youn, C. Lee, H. W. Kang, K. M. Kim, and K. C. Dho, Oceans **2** (2), 593 (2004).
14. E. N. Kalenov, Acoust. Phys. **61** (2), 205 (2015).
15. Y. P. Lee, H. Freese, and W. W. Lee, in *Proc. IEEE ASAP 2004, 12th Annual Workshop on Adaptive Sensor Array Processing* (*Massachusetts Institute of Technology,* Cambridge, MA, March 16–18, 2004).
16. S. J. Chern and C. Y. Chang, IEEE Trans. Antennas Propag. **50** (8), 1138 (2002).
17. H. Cox and H. Lai, in *Proc. 38th Asilomar Conference on Signals, Systems and Computers* (IEEE Press, 2004), Vol. 2, Issue 2, p. 2355
18. Y. Doisy, L. Deruaz, and R. Been, IEEE Trans. Signal Process. **58** (8), 4195 (2010).